Annual variations in phytoplankton biomass driven by small-scale physical processes

Madhavan Girijakumari Keerthi, Channing J. Prend, Olivier Aumont, Marina Lévy

Annual variations in phytoplankton biomass driven by small-scale physical processes

M. G. Keerthi[1*], C. J. Prend[2], O. Aumont[1], M. Lévy[1]

[1] Sorbonne Université (CNRS/IRD/MNHN), LOCEAN-IPSL, Paris, France.

[2] Scripps Institution of Oceanography, La Jolla, CA, USA.

Nature Geoscience

Corresponding author: M G Keerthi (keerthi.madhavan-girijakumari@locean.ipsl.fr)

Phytoplankton biomass exhibits significant year-to-year changes and understanding these changes is crucial to fisheries management and projecting future climate. These annual changes result partly from low-frequency climate modes that also lead to variations in sea surface temperature (SST). Here we evaluate the contribution of small scales to annual fluctuations based on a global analysis of satellite observations of sea surface chlorophyll (SChl), an indicator of phytoplankton biomass, and of SST, from 1999 to 2018. We disentangle the spatio-temporal scales of variability in the timeseries, and find that besides the prominent seasonal cycle, SChl is dominated by high-frequency fluctuations (<3 months) at small spatial scales (<50 km) —which accumulates over annual scales, in contrast to SST. The results suggest that observations and models with high spatio-temporal resolutions are necessary to understand annual changes in SChl. The rapid response of SChl to small-scale physical processes, combined with intrinsic ecosystem interactions and air-sea interaction feedbacks, may explain the differences between annual variations in SST and SChl.

Predicting the response of phytoplankton to climate change has important implications for biogeochemical cycling and ecosystem management[1-3] due to the key role phytoplankton play in marine food webs[4]. The continuous daily monitoring of surface chlorophyll-a (SChl), a proxy of phytoplankton biomass, from satellite radiometric measurements has been an invaluable tool to observe phytoplankton variability at the global scale over the past two decades[5-12]. As the satellite SChl timeseries grows, attempts have been made to detect climate change-driven trends[11-16]. However, this detection is made difficult by the large amplitude of natural variations, which overwhelm the long-term changes[16-18]. It is therefore essential to fully characterize natural SChl variability in order to attribute long-term changes to climate variability and/or anthropogenic forcing.

Because the primary mode of natural variability in SChl is the seasonal cycle[19], annual changes (i.e. changes from year-to-year) are the natural frame of reference for quantifying and attributing long-term trends. Previous attempts to explain year-to-year SChl changes have essentially focused on the role of large-scale, low-frequency climate modes; this has proved effective in the tropics. For example, climate modes such as El-Nino Southern Oscillation (ENSO) or the Indian Ocean Dipole (IOD) have been shown to explain most of phytoplankton variability in the tropical Pacific[20-23] and tropical Indian Ocean[24], respectively. But at higher latitudes, only modest correlations have been found between year-to-year SChl anomalies and the North Atlantic Oscillation[25,26] (NAO) or the Southern Annular Mode[27,28] (SAM).

Here we argue that annual changes in phytoplankton cannot be fully explained by climate modes because year-to-year SChl variations reflect processes occurring across a range of temporal scales from sub-seasonal to multi-annual. Satellite SChl timeseries indeed reveal that SChl fluctuations cover a large range of temporal scales, that can be shorter (sub-seasonal) or longer (multi-annual) than seasonality[6,19]. We quantify how fluctuations at sub-seasonal and seasonal frequencies, which are not necessarily related to climate modes, can lead to annual anomalies, and thus project onto the annual mean.

Sub-seasonal fluctuations in phytoplankton are large in many regions, with magnitudes that can be greater than twice the climatological mean[24,29-33]. For instance, over wide regions of the Southern Ocean[31] and along the deep convection zone of the Mediterranean Sea[34,35], the majority of SChl variance occurs at sub-seasonal timescales. In tropical cyclone-prone regions, synoptic-scale patches of increased productivity can account for 20-30% of the annual primary production[36]. These sub-seasonal SChl fluctuations are often the consequence of intermittency in surface

stratification, which can suppress or dilute the surface blooms or trigger transient phytoplankton growth by supplying nutrients to the euphotic zone[34,35,37,38]. Such high-frequency SChl fluctuations may be driven by sub-seasonal atmospheric variability including storms and (extra-) tropical cyclones[39-41], by sub-seasonal climate modes[24,43], or by mesoscale and sub-mesoscale eddies[44,45]. High-frequency SChl fluctuations may also reflect intrinsic variability in the biological system due to predator-prey interactions or resource competition[46,47]. All of these potential forcings operate over very different spatial scales, from <1 km in the case of intrinsic variability, 1-100 km for sub-mesoscale processes, 100-1000 km for cyclones and storms, to >1000 km for climate modes. Importantly, annual changes in eddy activity[48] or in the number of atmospheric storms[49], for instance, can alter annual mean SChl by influencing sub-seasonal SChl over the full year[50].

Seasonality in phytoplankton biomass is controlled by seasonal variations of solar irradiance, winds, and surface stratification, which modulate nutrient availability, light exposure and dilution rates[51-55]. The seasonal cycle is not strictly reproducible because the timing, number and magnitude of blooms vary from year-to-year[56,57]. Annual variability in the seasonal cycle (termed the delta-seasonal component hereafter) may be due to changes in the nutrient inventory and/or timing of mixed-layer shoaling, among other factors[56,57].

To demonstrate the contribution of sub-seasonal and delta-seasonal variations to annual changes, we decompose SChl timeseries over the global ocean into four distinct components: the annually repeating climatological seasonal component and three non-seasonal components, separated into sub-seasonal, delta-seasonal and multi-annual frequency ranges. Each non-seasonal component contributes to year-to-year changes. We evaluate the contribution of each non-seasonal component to the non-seasonal SChl variance. We also examine the associated spatial scales, which provide

information on the possible driving mechanism. We then repeat the same analysis for sea surface temperature (SST), another oceanic property observable by satellite at similar resolution for which longer timeseries are available. Trying to relate non-seasonal changes in SChl to those in SST is motivated by the fact that climate modes have a strong imprint on SST[58], and that phytoplankton distribution is modulated by some of the same transport processes as SST. However, we show that there are significant regional differences in the dominant temporal and spatial scales of SChl and SST non-seasonal variability. High-frequency subseasonal fluctuations dominate the non-seasonal part of SChl variability across vast regions of the ocean, and project onto the annual mean, while the low-frequency, multi-annual component governs SST. These results emphasize that sub-seasonal SChl events, and to a lesser extent delta-seasonal variations, should not be ignored when seeking to explain year-to-year changes in SChl or identify climate change-driven trends in primary productivity.

Decomposing SChl and SST temporal variations

We use the merged SChl product at 8-day temporal resolution distributed by European Space Agency Ocean Color Climate Change Initiative[59] (ESA OC-CCI), which gathers more than two decades of observations from multiple satellites and has good coverage (>70%) in most regions (Extended Data Fig. 1). For SST, we used the Optimum Interpolation Sea Surface Temperature (OISST) data distributed by NOAA, averaged over the same 8-day temporal grid as SChl. The amplitude of temporal SChl fluctuations varies at the global scale and mirrors the patterns in the annual mean (Extended Data Fig. 1). Namely, large values are observed in the high-latitude spring bloom regions, in boundary current regions and along the equator, where permanent and/or seasonal convection or upwelling supply nutrients to the surface layer; conversely, low values are observed over the nutrient-poor subtropical gyres[15].

The magnitude of SChl fluctuations results from the combined variability across a range of timescales. In order to isolate these signals, we use an iterative band-pass filter algorithm[35] adapted from the census X11 technique[6] that separates local timeseries X_t into sub-seasonal (SS_t, ~0.5-3 months), seasonal (S_t, ~3-12 months) and multi-annual (MA_t, ~12-120 months) constituents, such that $X_t = SS_t + S_t + MA_t$ (see Methods). This method allows for small overlaps in the frequency ranges associated with each component to account for regional variations in the dominant frequencies of the seasonal cycle (some regions being dominated by one or two annual blooms, for example). The method also allows the seasonal constituent S_t to vary from year-to-year. Hence S_t can be further separated into a repeating climatological seasonal cycle CS_t and a residual delta-seasonal component defined as $\Delta S_t = S_t - CS_t$ which captures annual variations in the seasonal cycle (see Methods). At each grid cell, the local time-series is thus decomposed into four constituents $X_t = SS_t + \Delta S_t + CS_t + MA_t$. In the following, we examine the non-seasonal part of X_t, which we define as $NS_t = X_t - CS_t = SS_t + \Delta S_t + MA_t$, and which thus includes a sub-seasonal SS_t, a delta-seasonal ΔS_t and a multi-annual MA_t component. Extended Data Fig. 2 shows the decomposition at a station where the non-seasonal variability of SChl is particularly large. We can see that CS_t is positive, while SS_t, ΔS_t and MA_t oscillate around zero but have a non-zero annual mean; the annual mean of CS_t is constant and the annual means of SS_t, ΔS_t and MA_t vary from year-to-year. Extended Data Fig. 3 and 4 show examples of SChl and SST timeseries from different regions and their corresponding power spectra, illustrating the wide range of frequencies in their non-seasonal components.

Strikingly for SChl, the variance of the non-seasonal part NS_t exceeds the variance of the climatological seasonal part SC_t in many places (Fig. 1). For example, in some tropical and subpolar regions, non-seasonal variability contributes more than 70% of the total SChl variance

(Fig. 1a). Also, notably, the non-seasonal part of SST variability is much smaller (generally <20%) than that of SChl, except in the equatorial region (Fig. 1b). In the following, we examine the relative contribution of each of the three components of the non-seasonal SChl and SST variability, bearing in mind that the non-seasonal variance is much larger for SChl than for SST.

Non-seasonal SChl and SST variability

The relative contribution of each component to the non-seasonal SChl and SST variance exhibits clear regional and latitudinal patterns (Fig. 2). In most regions, non-seasonal SChl variability is dominated (>50%) by the sub-seasonal component, whereas non-seasonal SST variability is dominated by its multi-annual component (>40%). For SChl, delta-seasonal variations explain only a small part of the non-seasonal variance (~10-20%). Multi-annual SChl variations are also generally modest and account for less than 30% of the non-seasonal variance in most locations. A notable exception to this is in the tropical Pacific, where multi-annual fluctuations largely dominate over the well-known horseshoe pattern of ENSO[9]; this is also reflected in the region's SST variability (Fig. 2c,g). Despite this, when averaged over the entire tropical band (20°N-20°S), multi-annual variability contributes less to the non-seasonal SChl variance (~25%) than the sub-seasonal (~50%) component (Fig. 2d). Compared to SChl, sub-seasonal events contribute much less to the non-seasonal SST variance (Fig. 2e-h). Sub-seasonal SST variability is largest within western boundary currents, along the equator, and in the Indian Ocean, but elsewhere, the multi-annual component dominates the non-seasonal SST variance.

Next, we examine the spatial scales associated with each non-seasonal component of the decomposition (Fig. 3). We estimate these by computing the distance over which a signal remains self-coherent using cross-correlation (see Methods). For both SChl and SST, the largest spatial

scales correspond to the multi-annual component, and the smallest to the sub-seasonal component. This provides insight into the relevant forcings operating at each timescale. For example, in the tropics, the spatial scales associated with the multi-annual component (>500 km), are consistent with the scales of tropical climate modes (e.g. ENSO, IOD). The spatial scales of the delta-seasonal component are about ~100-200 km for SChl and ~200-400 km for SST, consistent with scales of year-to-year variations in stratification and radiative forcing (i.e. linked to spatial scales of atmospheric variability); they are smaller for SChl than for SST, reflecting differences in biological and thermal response to this physical forcing, such as the fact that phytoplankton phenology, unlike SST, may respond non-monotonically to changes in stratification[60].

The sub-seasonal component, on the other hand, has much smaller spatial scales, ~50 km for SChl and ~100-200 km for SST. These scales are consistent with variability driven by mesoscale and submesoscale eddies. Nevertheless, while frontal scales <100 km dominate the SChl sub-seasonal variance, there are locations where a significant portion has spatial scales >100 km (Extended Data Fig. 5). These regions are primarily found at high-latitudes where the larger scales may reflect synoptic storms[32,41] and in the tropics where they may reflect intraseasonal climate modes such as Madden Julian Oscillation[61,62], Kelvin waves[63], or tropical instability waves[64].

The differences between SST and SChl sub-seasonal variations in both spatial scale and relative magnitude are striking given that both are influenced by the same ocean circulation and mixing. However, there are several elements that can explain these differences. First of all, those same dynamics act over different tracer gradients. It is likely that phytoplankton concentration is more sensitive to vertical exchanges than is SST because of the strong vertical gradients of phytoplankton and nutrients resulting from the fact that photosynthesis is limited to the euphotic layer. It has been

observed that SChl is particularly sensitive to episodic nitrate injection over fronts and frontal areas between eddies[65] with relative changes of order 40% for SChl but less than 5% for SST[66]. On the other hand, both SST and SChl anomalies are observed in the core of eddies[67]. This is consistent with the spatial scales for sub-seasonal variability (Fig. 3), which are closer to the frontal/submesoscale/mesoscale for SChl and to the mesoscale for SST. Another factor that might generate SChl sub-seasonal variations (but not SST) are ecological processes. For instance, predator-prey interactions[68], resource competition[69], and the interplay between the two[46], can lead to oscillations in phytoplankton biomass on short timescales (<3 months). On the other hand, air-sea heat fluxes could damp the variability for SST; for example, through the air-sea turbulent heat flux feedback over mesoscale eddies, which has been recently identified in high resolution coupled ocean-atmosphere models[70,71] and quantified[72]. This effect could contribute to part of the differences observed in both the sub-seasonal and delta-seasonal components. In summary, the strong contribution of sub-seasonal variations, unique to SChl, may reflect submesoscale-driven vertical exchanges[73-75], amplified by storm-driven mixing[76,77] and the effects of ecological processes, while the much weaker sub-seasonal SST variations may be the consequence of damping by air-sea fluxes.

Implications for year-to-year and longer-term variations

Year-to-year fluctuations in SChl are largely captured by the multi-annual component of SChl, but our result show that sub-seasonal and delta-seasonal fluctuations also contribute to variations in the annual mean. To quantify their relative importance, we define an annual mean low-frequency index as the correlation between annual mean SChl and the annual mean multi-annual component of SChl (Fig. 4). The index is close to one where annual mean changes are governed by low-frequency variations (>1 year, i.e. multi-annual). The index decreases as variability at higher

frequencies (<1 year, i.e. sub-seasonal plus delta-seasonal) contributes to the annual mean changes. For SChl, we find that the index is close to one in parts of the tropics and subtropics but decreases (down to 0.5) in the equatorial Atlantic and subpolar regions where sub-seasonal variability and an irregular seasonal cycle become larger. Notably, the regions where high-frequency variability contributes the most to year-to-year variations are those where the eddy and frontal activity are known to be large, such as in the Southern Ocean, in Western boundary current regions, or in Eastern boundary upwelling systems. Thus, across large swaths of the global ocean, year-to-year changes in SChl are not synonymous with low-frequency variability. Our result contrast with previous understanding of SChl year-to-year changes, which have often conflated year-to-year changes with low-frequency variability[9,23,26,28,78]. We should emphasize that previous studies have not necessarily precluded the influence of high-frequency variability, but rather have assumed that the combined effect of short-term variability is one manifestation of climate modes. Indeed, there is growing evidence that the intensity of submesoscale circulations is modulated by large-scale climate modes[79-82]. But our results demonstrate the importance of the intrinsic chaotic nature of small-scale physical[84-86] and biological[87-89] oceanic processes that can project onto timescales longer than a year with no correlation to climate modes. Our analysis provides a global quantification of this more chaotic contribution of small spatio-temporal scales of variability to year-to-year changes in SChl.

In contrast to SChl, the annual mean low-frequency index computed for SST is close to one everywhere (global average of 0.987), which means that year-to-year changes in annual mean SST are primarily driven by low-frequency variability. This suggests that attempts to extend SChl timeseries beyond the satellite ocean color record using SST as a predictor variable[7,89,90] may be biased, particularly in extra-tropical regions. Previous studies have successfully reconstructed SChl

variability from SST in the tropical Pacific[90], which is a region of weak sub-seasonal SChl variability. But our results imply that SST cannot be used to project SChl temporal variability in places, such as high latitude and subpolar oceans, where sub-seasonal SChl variance is large.

Much of what we know about decadal and longer-term trends in primary productivity relies on biogeochemical models. Based on our results, there is an urgent need to evaluate the capabilities of the most recent models to simulate sub-seasonal variability, an aspect that, to our knowledge, has not received much attention. If our models fail to reproduce sub-seasonal SChl fluctuations, their ability to capture year-to-year variability and long-term trends is likely biased due to the role of high-frequency events in determining the annual mean values. Future work should also explore how changes in the prevalence of extreme atmospheric events, such as heat waves, storms, and tropical cyclones, which are predicted as a result of climate change[49,91-93], together with ocean mesoscale and submesoscale activity, whose intensity is also projected to be modified in a warmer ocean[81,94], might affect long-term changes in SChl. Such changes would project onto sub-seasonal variability, although being driven by anthropogenic forcing. Thus, our results suggest that high-frequency events must be considered and understood in the context of detecting long-term trends and understanding the response of phytoplankton to climate change.

Acknowledgments

The authors acknowledge the support from ANR-SOBUMS (Agence Nationale de la Recherché, contract number: ANR-16-CE01-0014) and CNES for this research. MGK is supported by a postdoctoral fellowship from CNRS (Centre National de la Recherche Scientifique). CJP is supported by a National Science Foundation Graduate Research Fellowship under Grant DGE-

1650112 and a Chateaubriand Fellowship from the Office for Science & Technology of the Embassy of France in the United States.

Author contribution

MGK, ML and OA conceived and developed the study. MGK performed the data analysis and made the plots. MGK, OA, ML & CJP made the interpretation of the results. CJP, ML, OA and MGK wrote the manuscript. ML revised the manuscript; MGK revised the figures. ML and OA supervised the whole research.

Competing interests statement: The authors declare no competing interests.

Figure Legends:

Figure 1: Seasonal and nonseasonal variance of SChl and SST. (Left Column) (a) Percentage of SChl variance explained by its nonseasonal (NS_t) components and **(b)** Percentage of SChl variance explained by its seasonal (S_t) and nonseasonal (NS_t) components in each latitudinal band. **(Right Column)** Same for SST

Figure 2: Time-scale decomposition of nonseasonal variance. (Left Column) Percentage of the nonseasonal SChl variance explained by its **(a)** Sub-seasonal (SS_t), **(b)** year to year varying seasonal (ΔS_t), and **(c)** Multi-annual (MA_t) components. **(d)** Percentage of the nonseasonal SChl variance explained by its three components in each latitudinal band. **(Right Column)** Same for SST.

Figure 3: Spatial scales of nonseasonal variations. Boxplot showing the spatial scales associated

to sub-seasonal (SS_t, yellow), delta- seasonal (ΔS_t, green), and multi-annual (MA_t, blue) variations in different latitudinal bands for **(a)** SChl and **(b)** SST. The black line within each box denotes the median, the limits of the box represent the 25th and 75th percentiles, and the lines extending above and below represent the 10th and 90th percentile. The sample size (n) in each latitudinal band is greater than 500.

Figure 4: Small spatio-temporal scales can drive annual variations in SChl. Annual mean low-frequency index for SChl, which is defined as the correlation square between annual mean and annual mean of the multi-annual component. When the index is close to one, year-to-year fluctuations in the annual mean reflect low frequency variability. The value of the index decreases as high-frequency variability (i.e., with timescales < 1 year, delta-seasonal plus subseasonal) contributes more to year-to-year variations. Thus, small spatio-temporal scales contribute the most to annual variations in SChl in dark blue regions.

References

1. Hays, G. C., Richardson, A. J. & Robinson, C. Climate change and marine plankton. Trends in ecology & evolution, 20(6), 337-344 (2005).
2. Doney, S. C. et al., Climate change impacts on marine ecosystems. Annual review of marine science, 4, 11-37 (2012).
3. IPCC Special Report on the Ocean and Cryosphere in a Changing Climate (H.-O. Pörtner, D.C. Roberts, V. Masson-Delmotte, P. Zhai, M. Tignor, E. Poloczanska, K. Mintenbeck, A. Alegría, M. Nicolai, A. Okem, J. Petzold, B. Rama, N.M. Weyer (eds.)), (2019).
4. Field, C. B., Behrenfeld, M. J., Randerson, J. T. & Falkowski, P. Primary production of the biosphere: integrating terrestrial and oceanic components. Science, 281(5374), 237-240 (1998).

5. Dandonneau, Y. et al. Seasonal and interannual variability of ocean color and composition of phytoplankton communities in the North Atlantic, equatorial Pacific and South Pacific. Deep Sea Research Part II: Topical Studies in Oceanography, 51(1-3), 303-318 (2004).
6. Vantrepotte, V. & Mélin, F. Temporal variability of 10-year global SeaWiFS time-series of phytoplankton chlorophyll a concentration. ICES Journal of Marine Science, 66(7), 1547-1556 (2009).
7. Martinez, E., Antoine, D., D'Ortenzio, F. & Gentili, B. Climate-driven basin-scale decadal oscillations of oceanic phytoplankton. Science, 326(5957), 1253-1256 (2009).
8. Frajka-Williams, E. & Rhines, P. B. Physical controls and interannual variability of the Labrador Sea spring phytoplankton bloom in distinct regions. Deep Sea Research Part I: Oceanographic Research Papers, 57(4), 541-552 (2010).
9. Vantrepotte, V. & Mélin, F. Inter-annual variations in the SeaWiFS global chlorophyll a concentration (1997–2007). Deep Sea Research Part I: Oceanographic Research Papers, 58(4), 429-441 (2011).
10. Ferreira, A. S. A., Hátún, H., Counillon, F., Payne, M. R. & Visser, A. W. Synoptic-scale analysis of mechanisms driving surface chlorophyll dynamics in the North Atlantic. Biogeosciences, 12(11), 3641-3653 (2015).
11. Gregg, W. W. & Rousseaux, C. S. Decadal trends in global pelagic ocean chlorophyll: A new assessment integrating multiple satellites, in situ data, and models. Journal of Geophysical Research: Oceans, 119(9), 5921-5933 (2014).
12. Gregg, W. W. & Rousseaux, C. S. Global ocean primary production trends in the modern ocean color satellite record (1998–2015). Environmental Research Letters, 14(12), 124011, (2019).

13. Antoine, D., Morel, A., Gordon, H. R., Banzon, V. F. & Evans, R. H. Bridging ocean color observations of the 1980s and 2000s in search of long-term trends. Journal of Geophysical Research: Oceans, 110(C6), (2005).
14. Behrenfeld, M. J. et al. Climate-driven trends in contemporary ocean productivity. Nature, 444(7120), 752-755 (2006).
15. Siegel, D. A. et al. Regional to global assessments of phytoplankton dynamics from the SeaWiFS mission. Remote Sensing of Environment, 135, 77-91 (2013).
16. Henson, S. A. et al. Detection of anthropogenic climate change in satellite records of ocean chlorophyll and productivity. Biogeosciences, 7(2), 621-640 (2010).
17. Beaulieu, C. et al. Factors challenging our ability to detect long-term trends in ocean chlorophyll. Biogeosciences, 10(4), 2711-2724 (2013).
18. Henson, S. A., Beaulieu, C. & Lampitt, R. Observing climate change trends in ocean biogeochemistry: when and where. Global change biology, 22(4), 1561-1571 (2016).
19. Demarcq, H., Reygondeau, G., Alvain, S. & Vantrepotte, V. Monitoring marine phytoplankton seasonality from space. Remote sensing of environment, 117, 211-222 (2012).
20. Wilson, C. & Adamec, D. Correlations between surface chlorophyll and sea surface height in the tropical Pacific during the 1997–1999 El Niño-Southern Oscillation event. Journal of Geophysical Research: Oceans, 106(C12), 31175-31188 (2001).
21. Chavez, F. P. et al. Biological and chemical consequences of the 1997–1998 El Niño in central California waters. Progress in Oceanography, 54(1-4), 205-232 (2002).
22. Nababan, B., Muller-Karger, F. E., Hu, C. & Biggs, D. C. Chlorophyll variability in the northeastern Gulf of Mexico. International Journal of Remote Sensing, 32(23), 8373-8391 (2011).
23. Racault, M. F. et al. Impact of El Niño variability on oceanic phytoplankton. Frontiers in Marine Science, 4, 133 (2017).

24. Resplandy, L., Vialard, J., Lévy, M., Aumont, O. & Dandonneau, Y. Seasonal and intraseasonal biogeochemical variability in the thermocline ridge of the southern tropical Indian Ocean. Journal of Geophysical Research: Oceans, 114(C7), (2009).
25. Resplandy, L., Vialard, J., Lévy, M., Aumont, O. & Dandonneau, Y. Seasonal and intraseasonal biogeochemical variability in the thermocline ridge of the southern tropical Indian Ocean. Journal of Geophysical Research: Oceans, 114(C7), (2009).
26. Martinez, E., Raitsos, D. E. & Antoine, D. Warmer, deeper, and greener mixed layers in the North Atlantic subpolar gyre over the last 50 years. Global change biology, 22(2), 604-612 (2016).
27. Dutkiewicz, S., Follows, M., Marshall, J. & Gregg, W. W. Interannual variability of phytoplankton abundances in the North Atlantic. Deep Sea Research Part II: topical studies in oceanography, 48, 2323–2344 (2001).
28. Lovenduski, N. S. & Gruber, N. Impact of the Southern Annular Mode on Southern Ocean circulation and biology. Geophysical Research Letters, 32(11), (2005).
29. Prend,C.J., Keerthi, M.G., Levy, M., Aumont, O., Gille, S.T. & Talley, L.D. Sub-seasonal forcing drives year-to-year variations of Southern Ocean primary productivity, Global Biogeochemical Cycles, 36(7), e2022GB007329, (2022).
30. Bonhomme, C., Aumont, O. & Echevin, V. Advective transport caused by intraseasonal Rossby waves: A key player of the high chlorophyll variability off the Peru upwelling region. Journal of Geophysical Research: Oceans, 112(C9), (2007).
31. Fauchereau, N., Tagliabue, A., Bopp, L. & Monteiro, P. M. The response of phytoplankton biomass to transient mixing events in the Southern Ocean. Geophysical Research Letters, 38(17), (2011).

32. Thomalla, S. J., Fauchereau, N., Swart, S. & Monteiro, P. M. S. Regional scale characteristics of the seasonal cycle of chlorophyll in the Southern Ocean. Biogeosciences, 8(10), 2849-2866 (2011).
33. Strutton, P. G. et al. Biogeochemical variability in the central equatorial Indian Ocean during the monsoon transition. Biogeosciences, 12(8), 2367-2382 (2015).
34. Gomez, F. A., Spitz, Y. H., Batchelder, H. P. & Correa-Ramirez, M. A. Intraseasonal patterns in coastal plankton biomass off central Chile derived from satellite observations and a biochemical model. Journal of Marine Systems, 174, 106-118 (2017).
35. Keerthi, M. G., Levy, M., Aumont, O., Lengaigne, M. & Antoine, D. Contrasted contribution of intraseasonal time scales to surface chlorophyll variations in a bloom and an oligotrophic regime. Journal of Geophysical Research: Oceans, 125(5), e2019JC015701, (2020).
36. Keerthi, M. G., Lévy, M. & Aumont, O. Intermittency in phytoplankton bloom triggered by modulations in vertical stability. Scientific reports, 11(1), 1-9 (2021).
37. Menkes, C. E. et al. Global impact of tropical cyclones on primary production. Global Biogeochemical Cycles, 30(5), 767-786 (2016).
38. Lacour, L. et al. Unexpected winter phytoplankton blooms in the North Atlantic subpolar gyre. Nature Geoscience, 10, 836-839 (2017).
39. Carranza, M. M. et al. When mixed layers are not mixed. Storm-driven mixing and bio-optical vertical gradients in mixed layers of the Southern Ocean. Journal of Geophysical Research: Oceans, 123(10), 7264-7289 (2018).
40. Sanford, T. B., Price, J. F. & Girton, J. B. Upper-ocean response to Hurricane Frances (2004) observed by profiling EM-APEX floats. Journal of Physical Oceanography, 41(6), 1041-1056 (2011).

41. Carranza, M. M. & Gille, S. T. Southern Ocean wind-driven entrainment enhances satellite chlorophyll-a through the summer. Journal of Geophysical Research: Oceans, 120, 304-323 (2015).
42. Swart, S., Thomalla, S. J. & Monteiro, P. M. The seasonal cycle of mixed layer dynamics and phytoplankton biomass in the Sub-Antarctic Zone: A high-resolution glider experiment. Journal of Marine Systems, 147, 103-115 (2015).
43. Keerthi, M. G. et al. Intraseasonal variability of mixed layer depth in the tropical Indian Ocean. Climate dynamics, 46(7-8), 2633-2655 (2016).
44. Gaube, P., McGillicuddy Jr, D. J., Chelton, D. B., Behrenfeld, M. J., & Strutton, P. G. Regional variations in the influence of mesoscale eddies on near-surface chlorophyll. Journal of Geophysical Research: Oceans, 119(12), 8195-8220 (2014).
45. Hausmann, U., McGillicuddy Jr, D. J. & Marshall, J. Observed mesoscale eddy signatures in Southern Ocean surface mixed-layer depth. Journal of Geophysical Research: Oceans, 122(1), 617-635 (2017).
46. Mayersohn, B., Smith, K. S., Mangolte, I. & Lévy, M. Intrinsic timescales of variability in a marine plankton model. Ecological Modelling, 443, 109446, (2021).
47. Dakos, V., Beninca, E., van Nes, E. H., Philippart, C. J., Scheffer, M., & Huisman, J. Interannual variability in species composition explained as seasonally entrained chaos. Proceedings of the Royal Society B: Biological Sciences, 276(1669), 2871-2880 (2009).
48. Stammer, D., Wunsch, C., & Ueyoshi, K. Temporal changes in ocean eddy transports. Journal of Physical Oceanography, 36(3), 543-550 (2006).
49. Knutson, T. et al. Tropical cyclones and climate change assessment: Part II: Projected response to anthropogenic warming. Bulletin of the American Meteorological Society, 101(3), E303-E322, (2020).

50. Nicholson, S. A., Levy, M., Llort, J., Swart, S. & Monteiro, P. M. S. Investigation into the impact of storms on sustaining summer primary productivity in the Sub-Antarctic Ocean. Geophysical Research Letters, 43, 9192–9199 (2016).
51. Lévy, M. et al. Basin-wide seasonal evolution of the Indian Ocean's phytoplankton blooms. Journal of Geophysical Research: Ocean, 112, C12, (2007).
52. Echevin, V., Aumont, O., Ledesma, J. & Flores, G. The seasonal cycle of surface chlorophyll in the Peruvian upwelling system: A modelling study. Progress in Oceanography,79, 167–176 (2008).
53. Blain, S., Renaut, S., Xing, X., Claustre, H. & Guinet, C. Instrumented elephant seals reveal the seasonality in chlorophyll and light-mixing regime in the iron-fertilized Southern Ocean. Geophysical Research Letters, 40, 6368–6372 (2013).
54. Behrenfeld, M. J. & Boss, E. S. Resurrecting the ecological underpinnings of ocean plankton blooms. Annual review of marine science, 6, 167-194 (2014).
55. Sathyendranath, S., Ji, R. & Browman, H. I. Revisiting Sverdrup's critical depth hypothesis. ICES Journal of Marine Science, 72(6), 1892-1896 (2015).
56. Martinez, E., Antoine, D., d'Ortenzio, F., & de Boyer Montégut, C. Phytoplankton spring and fall blooms in the North Atlantic in the 1980s and 2000s. Journal of Geophysical Research: Oceans, 116(C11), (2011).
57. Ferrari, R., Merrifield, S. T. & Taylor, J. R. Shutdown of convection triggers increase of surface chlorophyll. Journal of Marine Systems, 147, 116–122 (2015).
58. Deser, C., Alexander, M. A., Xie, S. P., & Phillips, A. S. Sea surface temperature variability: Patterns and mechanisms. Annual review of marine science, 2, 115-143 (2010).
59. Sathyendranath, S. et al. An ocean-colour time series for use in climate studies: the experience of the Ocean-Colour Climate Change Initiative (OC-CCI). Sensors: 19, 4285, (2019).

60. Llort, J., Lévy, M., Sallée, J.-B. & Tagliabue, A. Nonmonotonic Response of Primary Production and Export to Changes in Mixed-Layer Depth in the Southern Ocean. Geophys. Res. Lett. 46, 3368–3377 (2019).
61. Waliser, D. E., Murtugudde, R., Strutton, P. & Li, J. L. Subseasonal organization of ocean chlorophyll: Prospects for prediction based on the Madden-Julian oscillation. Geophysical Research Letters, 32(23), (2005).
62. Jin, D., Waliser, D. E., Jones, C. & Murtugudde, R. Modulation of tropical ocean surface chlorophyll by the Madden–Julian Oscillation. Climate dynamics, 40(1-2), 39-58 (2013).
63. Xu, T., Li, S., Hamzah, F., Setiawan, A., Susanto, R. D., Cao, G. & Wei, Z. Intraseasonal flow and its impact on the chlorophyll-a concentration in the Sunda Strait and its vicinity. Deep-Sea Research I, 136, 84-90 (2018).
64. Strutton, P. G., Ryan, J. P., & Chavez, F. P. Enhanced chlorophyll associated with tropical instability waves in the equatorial Pacific. Geophysical Research Letters, 28(10), 2005-2008 (2001).
65. Wilson, C. Evidence of Episodic Nitrate Injections in the Oligotrophic North Pacific associated with Surface Chlorophyll Blooms. Journal of Geophysical Research: Oceans, 126(11), e2021JC017169, (2021).
66. Liu, X., & Levine, N. M. Enhancement of phytoplankton chlorophyll by submesoscale frontal dynamics in the North Pacific Subtropical Gyre. Geophysical Research Letters, 43, 1651– 1659 (2016).
67. The MODE group. The mid-ocean dynamics experiment. Deep Sea Res. 25, 859–910 (1978).
68. Fussmann, G.F., Ellner, S.P., Shertzer, K.W., & Hairston, Jr., N.G., Crossing the hopf bifurcation in a live predator-prey system. Science 290 (5495), 1358–1360 (2000).

69. Huisman, J., & Weissing, F.J., Biodiversity of plankton by species oscillations and chaos. Nature, 402 (6760), 407–410 (1999).

70. Small, R. J., Bryan, F. O., Bishop, S. P., Larson, S. & Tomas, R. A. What Drives Upper-Ocean Temperature Variability in Coupled Climate Models and Observations? J. Climate 33, 577–596 (2020).

71. Strobach, E. et al. Local Air-Sea Interactions at Ocean Mesoscale and Submesoscale in a Western Boundary Current. Geophys. Res. Lett. 49, e2021GL097003, (2022).

72. Moreton, S., Ferreira, D., Roberts, M. & Hewitt, H. Air-Sea Turbulent Heat Flux Feedback Over Mesoscale Eddies. Geophys. Res. Lett. 48, e2021GL095407 (2021).

73. Lévy, M., Ferrari, R., Franks, P. J., Martin, A. P., & Rivière, P. Bringing physics to life at the submesoscale. Geophysical Research Letters, 39(14), (2012).

74. Mahadevan, A. The impact of submesoscale physics on primary productivity of plankton. Annual review of marine science, 8, 161–184 (2016).

75. McWilliams, J. C. Submesoscale currents in the ocean. Proceedings of the Royal Society A: Mathematical, Physical and Engineering Sciences, 472(2189), 20160117, (2016).

76. Whitt, D. B., Taylor, J. R. & Lévy, M. Synoptic-to-planetary scale wind variability enhances phytoplankton biomass at ocean fronts. Journal of Geophysical Research: Ocean 122, 4602–4633 (2017).

77. Whitt, D. B., Lévy, M. & Taylor, J. R. Low-frequency and high-frequency oscillatory winds synergistically enhance nutrient entrainment and phytoplankton at fronts. Journal of Geophysical Research: Ocean, 122, 1016–1041 (2017).

78. Rousseaux, C. S. & Gregg, W. W. Interannual variation in phytoplankton primary production at a global scale. Remote Sensing, 6(1), 1-19 (2014).

79. Busecke, J. J., & Abernathey, R. P. Ocean mesoscale mixing linked to climate variability. Science Advances, 5(1), eaav5014, (2019).

80. Sasaki, H., Qiu, B., Klein, P., Sasai, Y., & Nonaka, M. Interannual to Decadal Variations of Submesoscale Motions around the North Pacific Subtropical Counter current. Fluids, 5(3), 116, (2020).

81. Richards, K. J., Whitt, D. B., Brett, G., Bryan, F. O., Feloy, K., & Long, M. C. The impact of climate change on ocean submesoscale activity. Journal of Geophysical Research: Oceans, 126(5), e2020JC016750, (2021).

82. Sasaki, H., Qiu, B., Klein, P., Nonaka, M., & Sasai, Y. Interannual Variations of Submesoscale Circulations in the Subtropical Northeastern Pacific. Geophysical Research Letters, e2021GL097664, (2022).

83. Arbic, B. K. et al. Geostrophic Turbulence in the Frequency–Wavenumber Domain: Eddy-Driven Low-Frequency Variability. J. Phys. Oceanogr. 44, 2050–2069 (2014).

84. Levy, M., Resplandy, L. & Lengaigne, M. Oceanic mesoscale turbulence drives large biogeochemical interannual variability at middle and high latitudes. Geophys. Res. Lett. 41, 2467–2474 (2014).

85. Sérazin, G. et al. A global probabilistic study of the ocean heat content low-frequency variability: Atmospheric forcing versus oceanic chaos. Geophys. Res. Lett. 44, 5580–5589 (2017).

86. Cravatte, S., Sérazin, G., Penduff, T. & Menkes, C. Imprint of chaotic ocean variability on transports in the southwestern Pacific at interannual timescales. Ocean Science 17, 487–507 (2021).

87. Huisman, J. & Weissing, F. J. Biodiversity of plankton by species oscillations and chaos. Nature 402, 407–410 (1999).

88. Benincà, E. et al. Chaos in a long-term experiment with a plankton community. Nature 451, 822–825 (2008).
89. Dunstan, P. K. et al. Global patterns of change and variation in sea surface temperature and chlorophyll a. Scientific reports, 8(1), 1-9 (2018).
90. Martinez, E. et al. Reconstructing global chlorophyll-a variations using a non-linear statistical approach. Frontiers in Marine Science, 7, 464, (2020).
91. Frölicher, T. L., Fischer, E. M., & Gruber, N. Marine heatwaves under global warming. Nature, 560(7718), 360-364 (2018).
92. Walsh, K. J. et al. Tropical cyclones and climate change. Wiley Interdisciplinary Reviews: Climate Change, 7(1), 65-89 (2016).
93. Shaw, T. A. et al. Storm track processes and the opposing influences of climate change. Nature Geoscience, 9(9), 656-664 (2016).
94. Martínez-Moreno, J. et al. Global changes in oceanic mesoscale currents over the satellite altimetry record. Nature Climate change, 1–7 (2021).

Methods

Sea-surface Chlorophyll (SChl) data: We use the Level 3 Mapped 25 x 25 km resolution 8-day averaged product (release 4.1) from January 1999 to December 2018 distributed by the European Space Agency Ocean Color Climate Change Initiative[95] (ESA OC-CCI; available at http://www.oceancolour.org/). This product merges data from several ocean color satellite missions: the Moderate Resolution Imaging Spectroradiometer (MODIS)-Aqua, the Sea-Viewing Wide Field-of-View Sensor (SeaWiFS), the MEdium Resolution Imaging Spectrometer (MERIS) and the Visible Infrared Imaging Radiometer Suite (VIIRS).

This product has good data coverage that exceeds 85% over most of the low and mid latitudes (Extended Data Fig. 1a). However, the coverage is lower in areas characterized by high annual or seasonal cloud cover such as the Intertropical Convergence Zone (ITCZ), Arabian Sea, and Bay of Bengal. Poleward of about 50° in both hemispheres, the data coverage rapidly falls below 60% and data availability becomes restricted mostly to the summer period as a consequence of the high solar angle, elevated cloudiness during winter and sea ice cover[96]. In view of these limitations, we restricted our analysis from 60°S to 60°N. Still, the merged ocean color product used here has better coverage, and extends over a longer time period, than any individual satellite product.

A further dilemma is whether the sub-seasonal SChl variability captured by the merged satellite product is reliable or is strongly aliased by noise/temporal under-sampling. Previous comparison with high-frequency in-situ mooring observations in the Mediterranean Sea revealed that the merged satellite product was accurate at sub-seasonal timescales[35], although it is unclear whether this holds true at other locations. It is also important to recognize that variations in SChl do not always reflect changes in depth-integrated biomass[39]. High-frequency, continuous, depth-resolved in-situ observations from a range of locations are needed to further characterize temporal variability in SChl and its relationship to net primary productivity.

Sea surface temperature (SST) data: We use the daily 25 x 25 km resolution Optimum Interpolation Sea Surface Temperature (OISST) data distributed by NOAA (available https://www.ncdc.noaa.gov/oisst/optimum-interpolation-sea-surface-temperature-oisst-v20) for the period January 1999 to December 2018. OISST data are constructed by combining observations from satellites, ships, buoys and Argo floats. SST was averaged over the same 8-day temporal grid as SChl.

Temporal decomposition: At each grid point, SChl and SST raw timeseries X_t were decomposed into four components $X_t = SS_t + \Delta S_t + CS_t + MA_t$. (sub-seasonal SS_t, delta-seasonal ΔS_t, climatological seasonal CS_t and multi-annual MA_t), in two steps. The first step is the decomposition method based on the Census X11 algorithm, which was initially developed by the U.S. Bureau of the Census[6] and adapted by Keerthi et al.,[35]. The first step ensures that $X_t = SS_t + S_t + MA_t$ at every location. The seasonal component (S_t) reflects variability with a period of 3 months to 1 year, while multi-annual component (MA_t) comprises variability with a timescale longer than 8 months. Finally, the sub-seasonal component (SS_t) captures variability in the 8-88 days frequency range, plus all irregular variability outside of that range. The X11 method requires continuous timeseries, thus gaps in the data were filled by linear interpolation in time before the application of the decomposition and were then masked. The filters used for the multi-annual component include a centered annual running average applied once, and a Henderson filter (of weight representative of a year) applied twice. The filters used for the seasonal component are a weighted running average over three consecutive 8-day timesteps of the given year and from the previous and consecutive years, applied twice, and an 88-day low-pass filter (corresponding to ~3 months given the 8-day resolution of the data).

In a second step, the seasonal constituent S_t is further separated into a repeating climatological seasonal cycle CS_t and a delta-seasonal component $S_t = CS_t. + \Delta S_t$. At each 8-day time step, CS_t is computed as the mean value of S_t over the 20 years of data. ΔS_t captures annual deviations in the seasonal cycle, such as different timing of blooms. The non-seasonal part of X_t, defined as $NS_t = X_t - C_t$ can thus be expressed as the exact sum of the sub-seasonal component (SS_t), the delta-seasonal component ($\Delta S_t.$) and the multi-annual component (MA_t).

Extended Data Fig. 2 shows an illustration of the decomposition of X_t for SChl in a station where the four components co-exist. Fourier power spectrum of each component show that there are several harmonics in the seasonal cycle, with frequencies from 3 months to over one year, that the frequency range of the sub-seasonal is less than one year, and that of the multi-annual component is more than 8 months. This illustrate that the X11 decomposition is not based on a clear frequency cut, in particular all components are present at a frequency close to 1 year. The frequency range of the seasonal component overlaps with the sub-seasonal on its high-frequency side, and with the multi-annual on its low frequency side. The advantage of iterative filtering over frequency cuts is that it captures the different harmonics of the seasonal cycle, which vary regionally[19], and adapts to them.

Variance explained: The total variance explained by the non-seasonal SChl timeseries is equal to the sum of the variance explained by its three different components, plus the covariance between these components. In practice, the covariance terms are small and we neglect them. The relative contribution of each component (delta-seasonal, multi-annual and sub-seasonal) to the non-seasonal variance is expressed as a percentage.

Spatial scale of coherence: It is defined as the spatial scale over which each component (delta-seasonal, multi-annual and sub-seasonal) remains self-coherent. In practice, we cross-correlated each component at a given grid cell with the same component at all other grid cells within a 300 km radius, and counted the number of grid cells for which the cross–correlation was larger than 0.8, and converted this number into a distance. The threshold value chosen here (0.8) is the same than in Keerthi et al.,[35].

Spatial decomposition: To quantify the relative contribution of spatial scales smaller than 100km

and larger than 100 km to the sub-seasonal signal, we performed a spatial decomposition at each time step. The spatial decomposition that we used is based on an iterative application of the heat diffusion equation described in Weaver and Courtier[97], and has been previously applied in Keerthi et al.[35,43,98].

Annual mean low-frequency index: It is defined as the correlation square between annual mean of the raw timeseries and annual mean of the multi-annual component.

$$\text{Annual mean low frequecy index} = \mathrm{r}^2\ (\overline{X_t}\ , \overline{\mathrm{MA_t}})$$

Where $\overline{X_t}$ is the annual (yearly) mean of the raw time series at each grid point and $\overline{\mathrm{MA_t}}$ is the annual (yearly) mean of the multi-annual component at each grid point.

All figures were generated with the SAXO package based on IDL (http://forge.ipsl.jussieu.fr/saxo/download/xmldoc/whatissaxo.html).

Data Availability: All data analyzed in this study are freely available from the respective websites mentioned in the Methods Section**.**

Methods-only references:

95. Sathyendranath. S. & Krasemann, H. Ocean Colour Climate Change Initiative (OC-CCI) — Phase one. Climate Assessment Report, (2014). http://www.esa-oceancolour-cci.org/?q=documents

96. Gregg, W. W. & Casey, N. W. Sampling biases in MODIS and SeaWiFS ocean chlorophyll data. Remote Sensing of Environment, 111(1), 25-35 (2007).

97. Weaver, A. & Courtier, P. Correlation modelling on the sphere using a generalized diffusion equation. Quarterly Journal of the Royal Meteorological Society, 127(575), 1815-1846 (2001).
98. Keerthi, M. G., Lengaigne, M., Vialard, J., de Boyer Montégut, C. & Muraleedharan, P. M. Interannual variability of the Tropical Indian Ocean mixed layer depth. Climate dynamics, 40(3), 743-759 (2013).

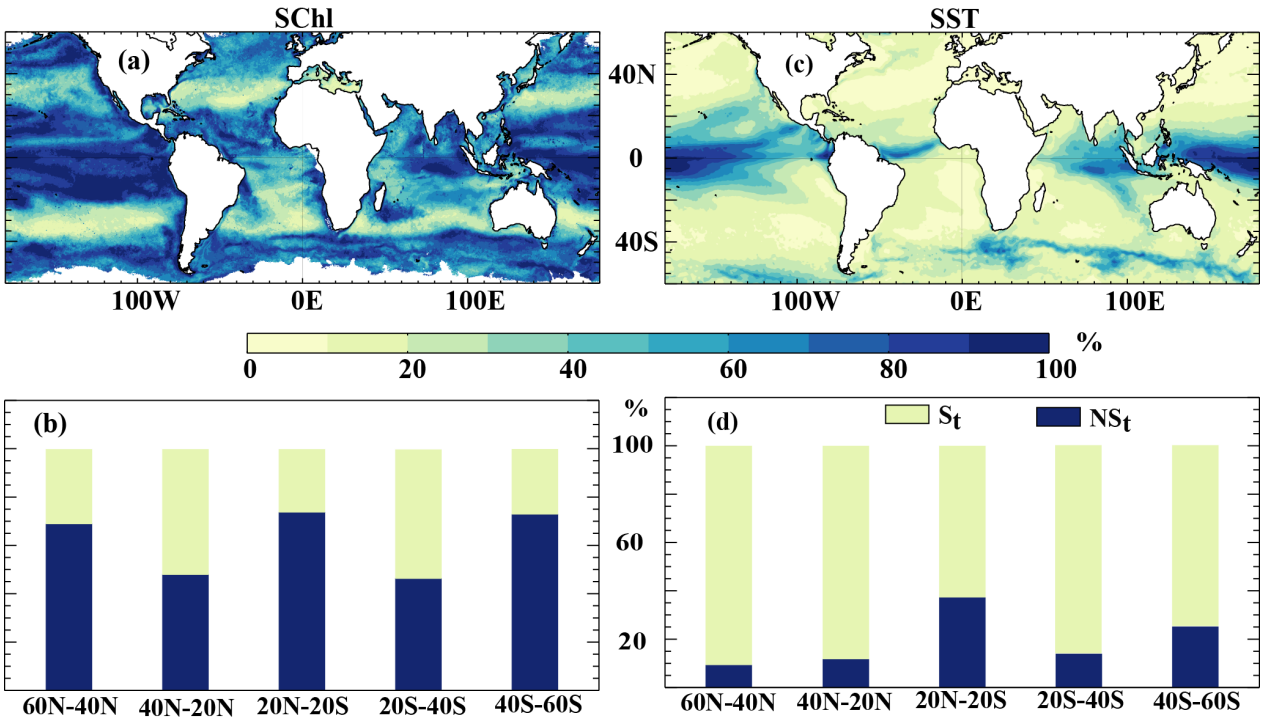

Figure 1: Seasonal and nonseasonal variance of SChl and SST. (Left Column) (a) Percentage of SChl variance explained by its nonseasonal (NS_t) components and **(b)** Percentage of SChl variance explained by its seasonal (S_t) and nonseasonal (NS_t) components in each latitudinal band. **(Right Column)** Same for SST

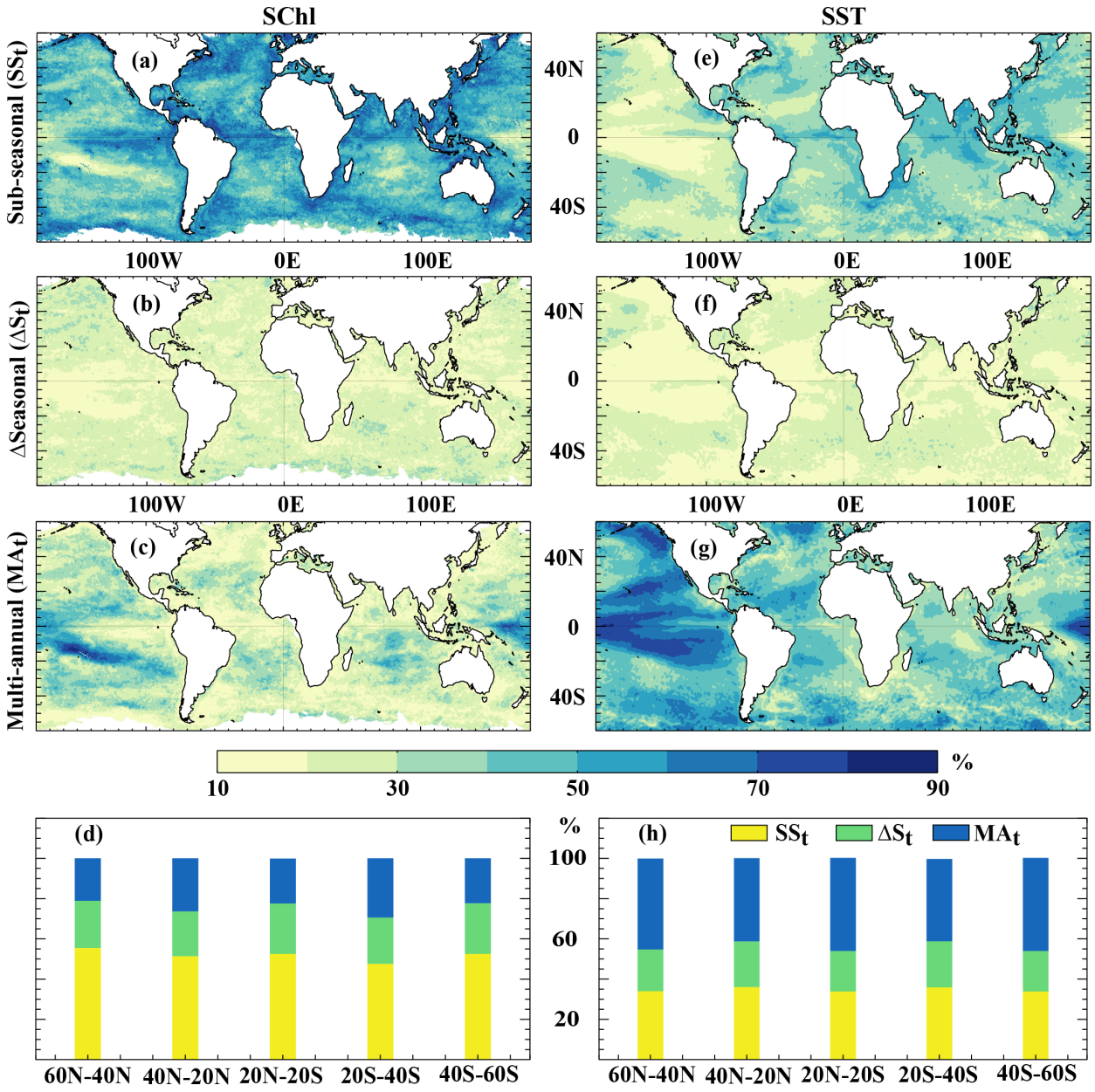

Figure 2: Time-scale decomposition of nonseasonal variance. (Left Column) Percentage of the nonseasonal SChl variance explained by its **(a)** Sub-seasonal (SS_t), **(b)** year to year varying seasonal (ΔS_t), and **(c)** Multi-annual (MA_t) components. **(d)** Percentage of the nonseasonal SChl variance explained by its three components in each latitudinal band. **(Right Column)** Same for SST.

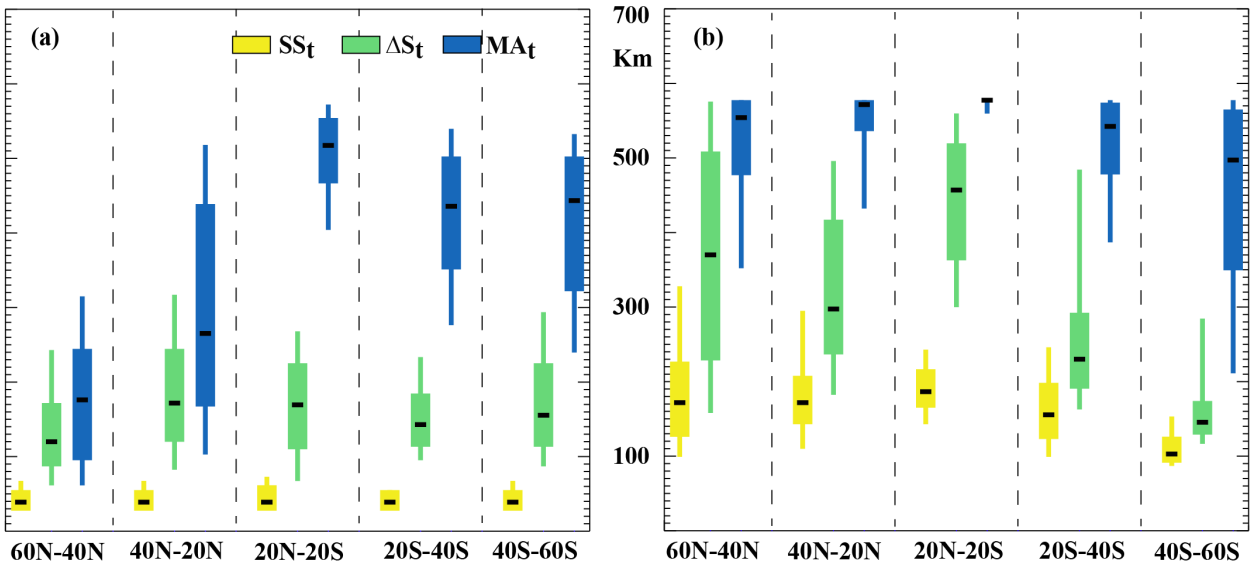

Figure 3: Spatial scales of nonseasonal variations. Boxplot showing the spatial scales associated to sub-seasonal (SS_t, yellow), delta- seasonal (ΔS_t, green), and multi-annual (MA_t, blue) variations in different latitudinal bands for **(a)** SChl and **(b)** SST. The black line within each box denotes the median, the limits of the box represent the 25th and 75th percentiles, and the lines extending above and below represent the 10th and 90th percentile. The sample size (n) in each latitudinal band is greater than 500.

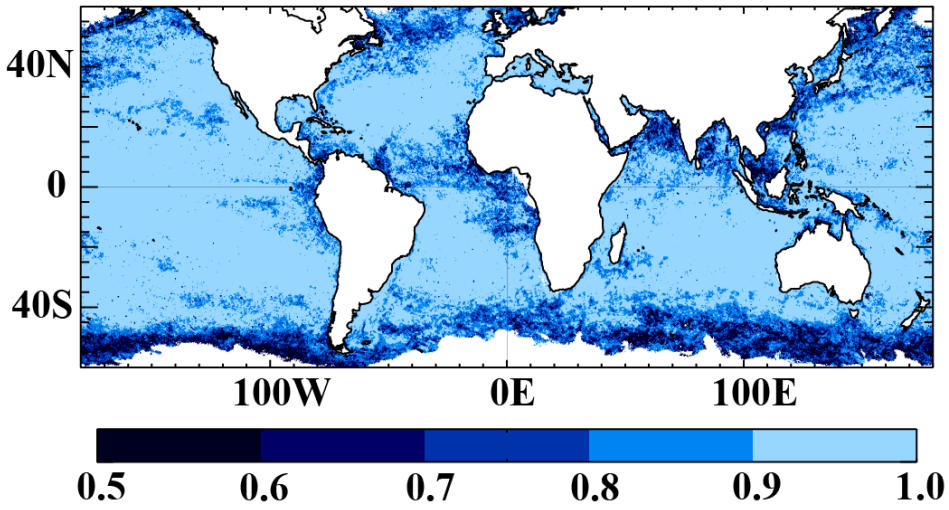

Figure 4: Small spatio-temporal scales can drive annual variations in SChl. Annual mean low-frequency index for SChl, which is defined as the correlation square between annual mean and annual mean of the multi-annual component. When the index is close to one, year-to-year fluctuations in the annual mean reflect low frequency variability. The value of the index decreases as high-frequency variability (i.e., with timescales < 1 year, delta-seasonal plus subseasonal) contributes more to year-to-year variations. Thus, small spatio-temporal scales contribute the most to annual variations in SChl in dark blue regions.

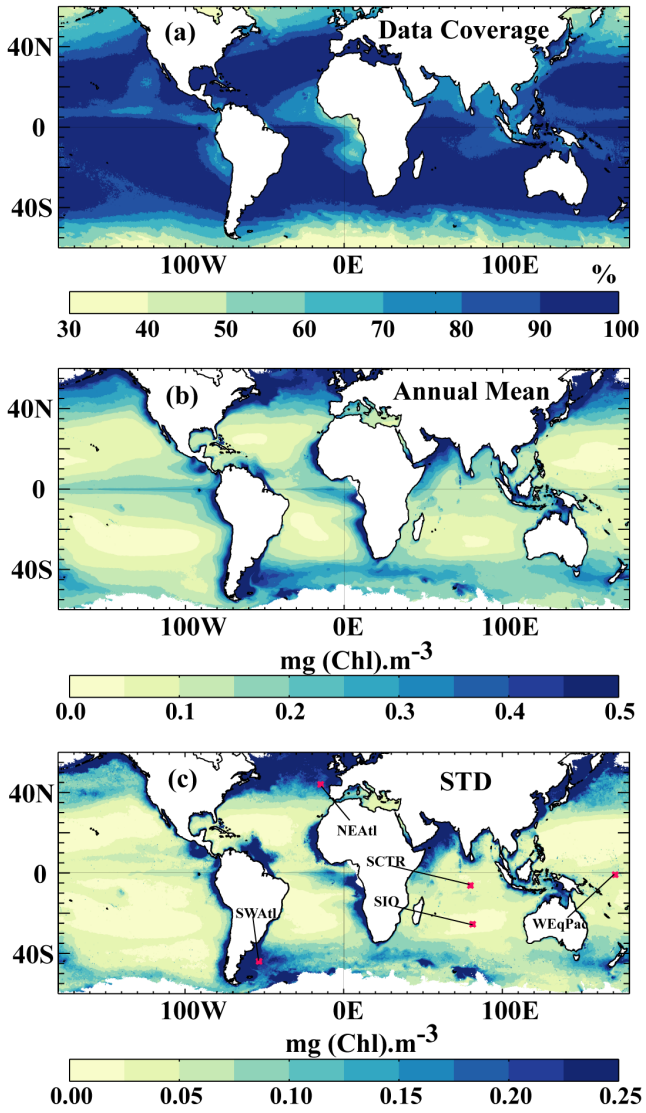

Extended Data Figure 1: SChl data distribution. SChl data coverage (percentage of time steps with data in each pixel with respect to the total number of time steps), (b) Annual mean and (c) Standard deviation, over the period 1999-2018.

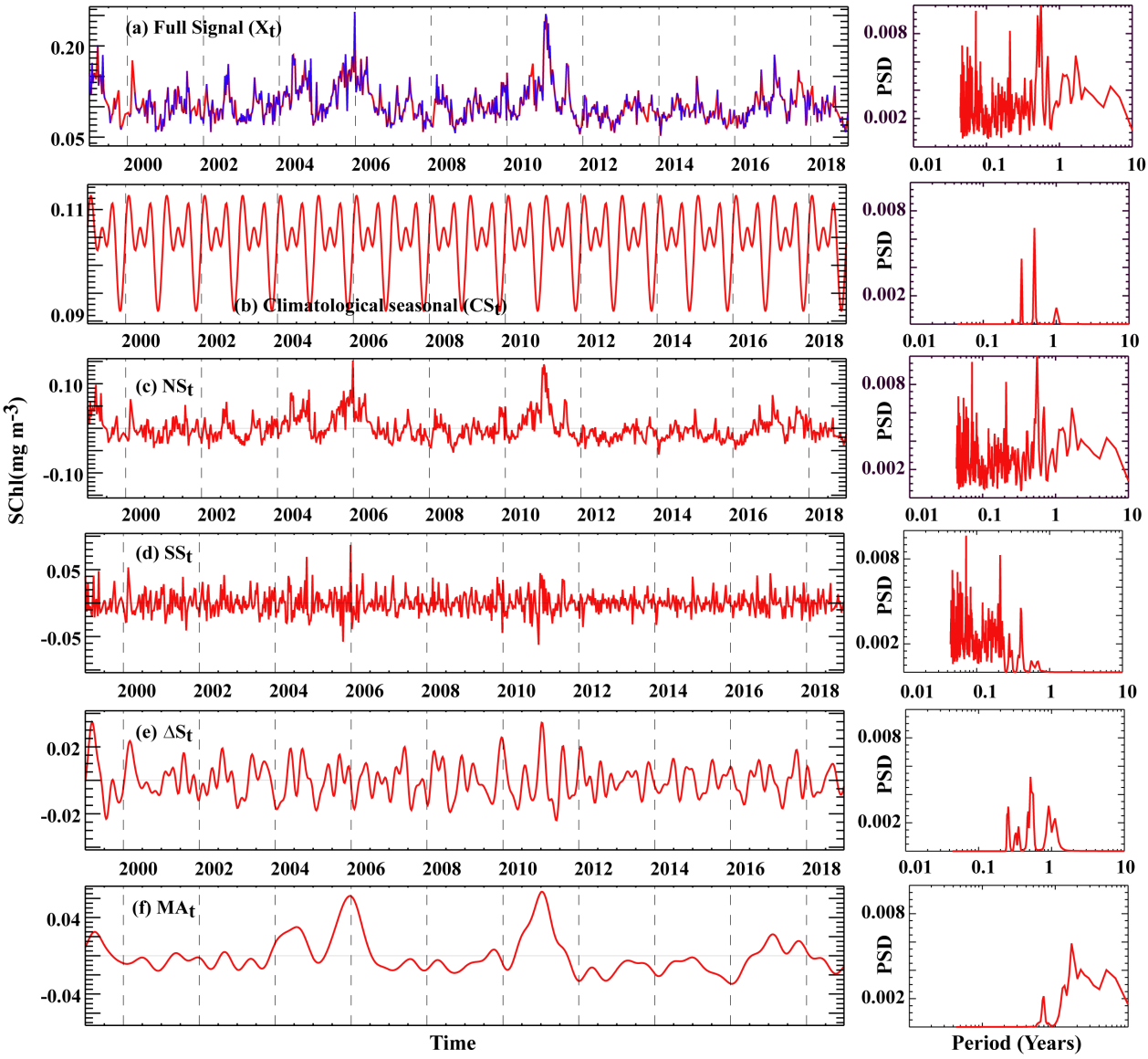

Extended Data Figure 2: Time series decomposition. (Left Panels) Decomposition of SChl timeseries at the Seychelles-Chagos Thermocline Ridge station (SCTR) - (a) full Signal X_t, (b) climatological seasonal cycle CS_t, (c) nonseasonal variability NS_t, and the different components of nonseasonal variability (d) sub-seasonal SS_t, (e) delta-seasonal ΔS_t and (f) multi-annual MA_t. In a), the blue curve shows the un-interpolated raw ESA OC-CCI SChl and the red curve shows the linearly interpolated SChl values. **(Right panels)** Associated power spectrum of the timeseries shown in the left panel. PSD is power spectral density. The SCTR station is marked on Supplementary Figure 1c.

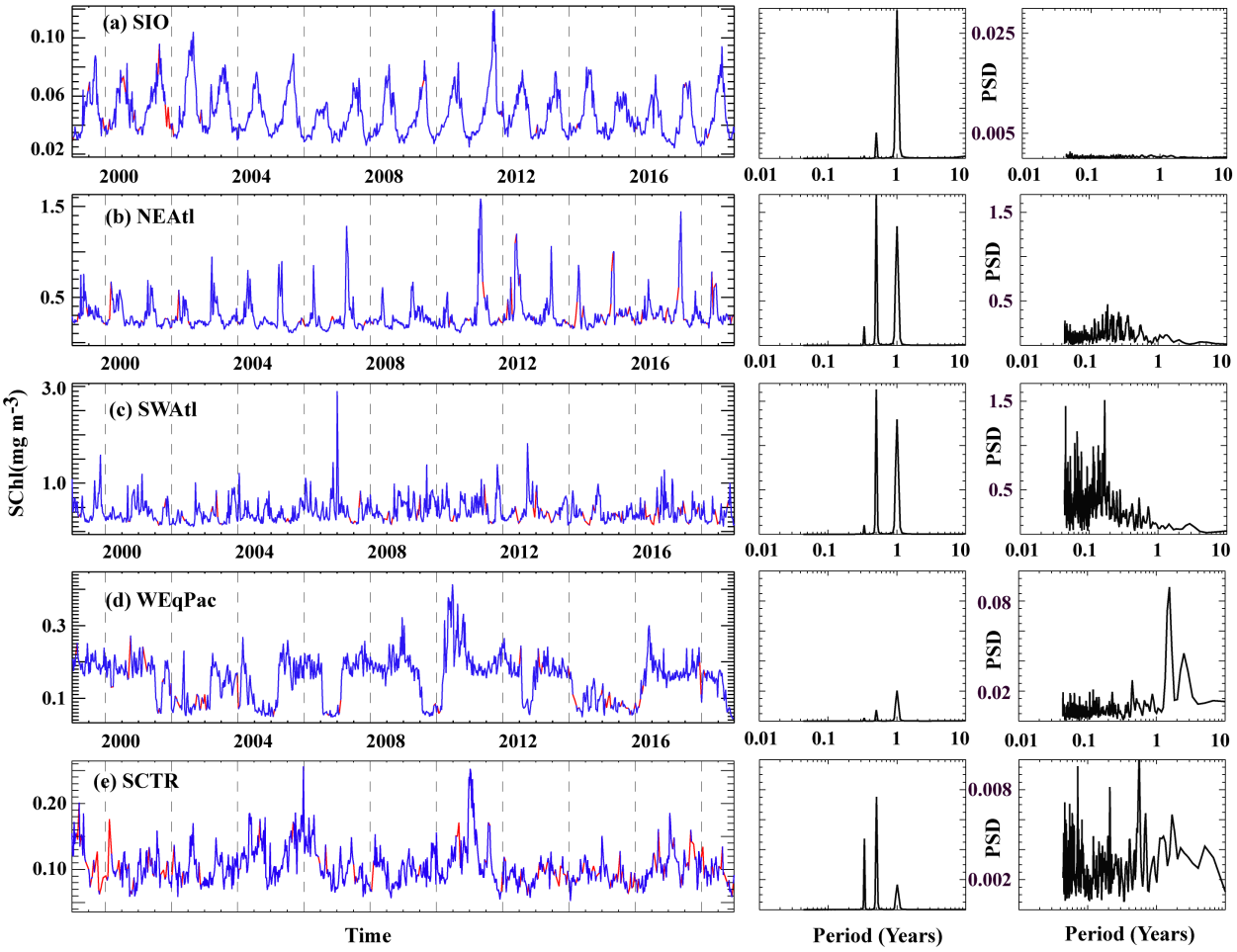

Extended Data Figure 3: SChl timeseries decomposition at specific locations. **(Left panels)** SChl time series for the stations marked in Supplementary Figure 1c. The blue curve shows the un-interpolated raw ESA OC-CCI SChl and the red curve denotes the linearly interpolated SChl on which the decomposition is applied. The power spectrum of the seasonal **(middle panels)** and non-seasonal **(right panels)** component for each station is shown. PSD is power spectral density.

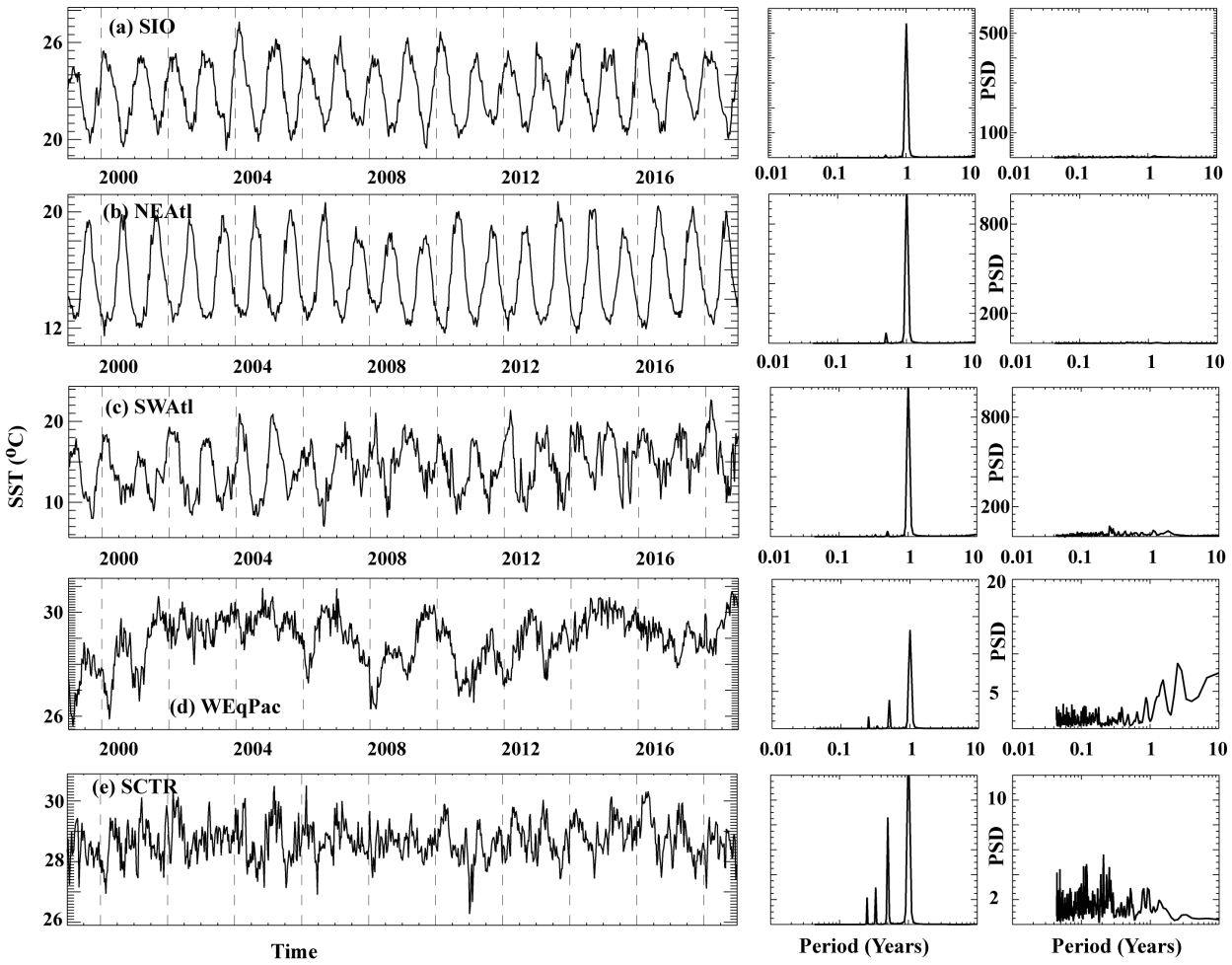

Extended Data Figure 4: SST timeseries decomposition at specific locations. Same as Extended Data Figure 3 but for SST.

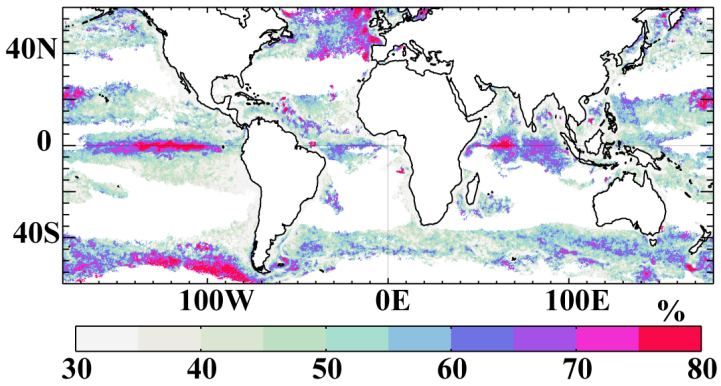

Extended Data Figure 5: Spatial scales of sub-seasonal SChl variations. Percentage of the sub-seasonal SChl variance explained by sub-seasonal variations with spatial scales >100 km. Regions where sub-seasonal variations explain less than 30% of the total SChl variance is masked.